ADVANCED MATERIALS
www.advmat.de

Dynamic Triboelectrification-Induced Electroluminescence and its Use in Visualized Sensing

*Xiao Yan Wei, Xiandi Wang, Shuang Yang Kuang, Li Su, Hua Yang Li, Ying Wang, Caofeng Pan, Zhong Lin Wang, and Guang Zhu**

Luminescence is a type of cold body radiation caused by external stimuli such as mechanical stress,[1–4] photoabsorption,[5,6] electric field,[7] and chemical reactions.[8] Distinct types of stimuli yield corresponding important applications that cover a wide spectrum of areas including lighting,[9,10] displays,[11] disinfection,[12] medical imaging,[13,14] and horticulture.[15,16] Here, we report a novel motion-driven luminescence. It is essentially a type of triboelectrification-induced electroluminescence (TIEL) that converts dynamic motions into luminescence upon extremely gentle mechanical interactions. The TIEL relies on the coupling between triboelectrification and electroluminescence (EL). Tribocharges resulting from relative dynamic interactions between two dissimilar materials can abruptly and significantly alter the surrounding electric potential by as high as hundreds of volts within milliseconds. Such a drastic change of the electric potential can excite the EL of underlying phosphor along the motion trajectory. The TIEL possesses prominent features. First, it is nondestructive to materials and thus has excellent stability, repeatability, and durability. Second, it can be excited by extremely weak stimuli. The threshold stress is as low as less than 10 kPa, three orders of magnitude smaller than that for elastico-triboluminescence (ETL); and the threshold velocity is less than 1 cm s^{-1}. Third, the stress responsivity in a low-stress region (<20 kPa) reaches up to 0.03 kPa^{-1}, presenting a 750-fold enhancement over the ETL. In addition, the light emission is achieved in atmospheric pressure instead of vacuum. As a demonstration of potential applications of this novel effect, position locating and motion tracking in a high-spatial resolution are achieved with the assistance of a software interface. Therefore, the TIEL is a new approach for a variety of applications including security surveillance, electronic commerce, anti-counterfeiting, and illumination.

In this work, a multilayered composite material is fabricated to investigate the TIEL. The composite comprises a substrate, a luminescent layer that consists of poly(methyl methacrylate) (PMMA) matrix and ZnS:Cu phosphor particles and an electrification layer made of fluorinated ethylene propylene (FEP), as shown in **Figure 1**a. Beginning with the substrate, they are sequentially constructed layer by layer. Figure 1b shows a cross-sectional view of the luminescent layer in a scanning electron microscopy (SEM) image. The average diameter of the phosphor particles is around 20 μm. Figure 1c shows X-ray diffraction pattern of the phosphor. Three major peaks at 2θ values of 28.82°, 48.31°, and 56.09° correspond to (111), (220), and (311) lattice planes of the zinc-blended structure.[17] Elementary analysis by energy-dispersive spectroscopy (EDS) in Figure 1d reveals the characteristic peak of Cu at 0.9 keV. A piece of the as-fabricated composite on a flexible polyimide (PI) substrate is displayed in Figure 1e. The detailed fabrication process is presented in the Experimental Section.

When a separate object slides against the electrification layer, transient light emission from the luminescent layer can be observed along the motion trajectory, as graphically shown in Figure 1a. To quantify the luminescence characteristics, we constructed a test platform, a diagram of which is shown in Figure S1 (Supporting Information). A pen-like object is used to rub the electrification layer, while an optic-fiber probe is in close proximity to the back of the substrate. It collects and directs the light emission to a spectrometer. The object and the probe are simultaneously driven by a linear stepper in a horizontal plane. Besides, a force sensor was installed at the back side of the substrate to monitor the vertical stress at the rubbing interface. As shown in **Figure 2**a, the obtained luminescence spectrum peaks at 510 nm, which corresponds to Commission Internationale de l'Éclairage (CIE) coordinates of (0.22, 0.49) (inset of Figure 2a).

For the ZnS:Cu phosphor, luminescence can be excited by stimuli including electric field, i.e., EL,[18–20] photons, i.e., photoluminescence (PL),[21–23] and stress, i.e., triboluminescence (TL).[24–26] In order to reveal the underlying mechanism of the measured luminescence, we prepared two control samples in which an extra layer was added between the luminescent layer and the electrification layer. As exhibited in Figure 2b, a layer of opaque black paint has little influence on the measured luminescence intensity, indicating that the observed light emission is not excited by photons in visible wavelength. In contrast, the luminescence vanishes if the extra layer is made from indium tin oxide (ITO)that is grounded. On one hand, the transparent ITO layer allows the transmission of either photons or stress, which excludes PL or TL as the possible mechanisms, respectively. On the other hand, the grounded ITO layer can shield the underlying luminescent layer from an electric field.

X. Y. Wei, X. Wang, S. Y. Kuang, Dr. L. Su, H. Y. Li, Y. Wang, Prof. C. Pan, Prof. Z. L. Wang, Prof. G. Zhu
Beijing Institute of Nanoenergy and Nanosystems
Chinese Academy of Sciences
National Center for Nanoscience and Technology (NCNST)
Beijing 100083, P. R. China
E-mail: zhuguang@binn.cas.cn
Prof. Z. L. Wang
School of Materials Science and Engineering
Georgia Institute of Technology
Atlanta, GA 30332, USA

DOI: 10.1002/adma.201600604

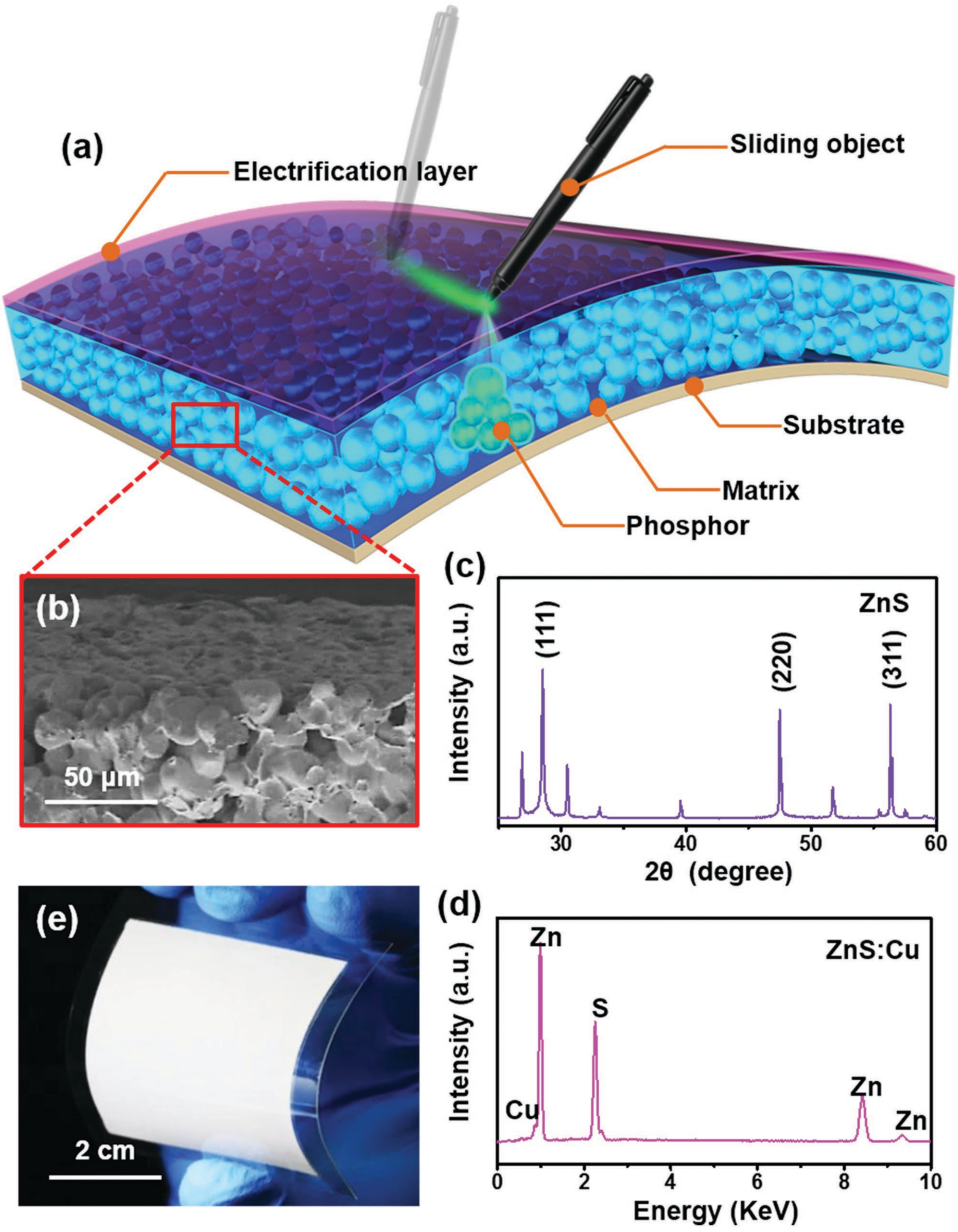

Figure 1. Structure of the TIEL composite material. a) Schematic of the layer-by-layer composite material and the induced luminescence along the sliding trajectory. b) SEM image of the luminescence layer showing ZnS:Cu particles imbedded in a PMMA matrix. c) X-ray diffraction pattern of the phosphor. d) EDS of the phosphor. e) Photograph of a bent composite on a flexible substrate.

Therefore, EL becomes the solely feasible reason that is accountable for the light emission. It is well known that contact between two dissimilar materials can produce tribocharges of opposite signs at the contact surfaces.[27–29] When the charged object laterally slides, it alters the surrounding distribution of electric potential along its motion trajectory; and the changing electric potential then excites the EL of the underlying phosphor.

The factors that can influence the luminescence intensity are investigated in two categories. From the aspect of internal factors, three parameters are discussed. First, the thickness of the electrification layer plays a decisive role in that the luminescence intensity exponentially increases as the thickness decreases, which is exhibited in Figure 2c. Second, the thickness of the phosphor layer has an optimal value (≈45 μm) for maximizing the luminescence intensity. As the phosphor layer becomes thicker, stronger light emission could be obtained due to more materials that are excited. However, excessively thick phosphor layer will block the escape of the emitted light, resulting in weakened intensity. Besides, surface morphology of the electrification layer is another important factor. Here, the electrification layer was pretreated by sandpaper rubbing. A rubbing cycle is defined as a reciprocating movement of the sandpaper against the electrification layer. As shown in Figure 2e, the luminescence intensity is substantially promoted as the rubbing cycle increases.

Adv. Mater. 2016,
DOI: 10.1002/adma.201600604

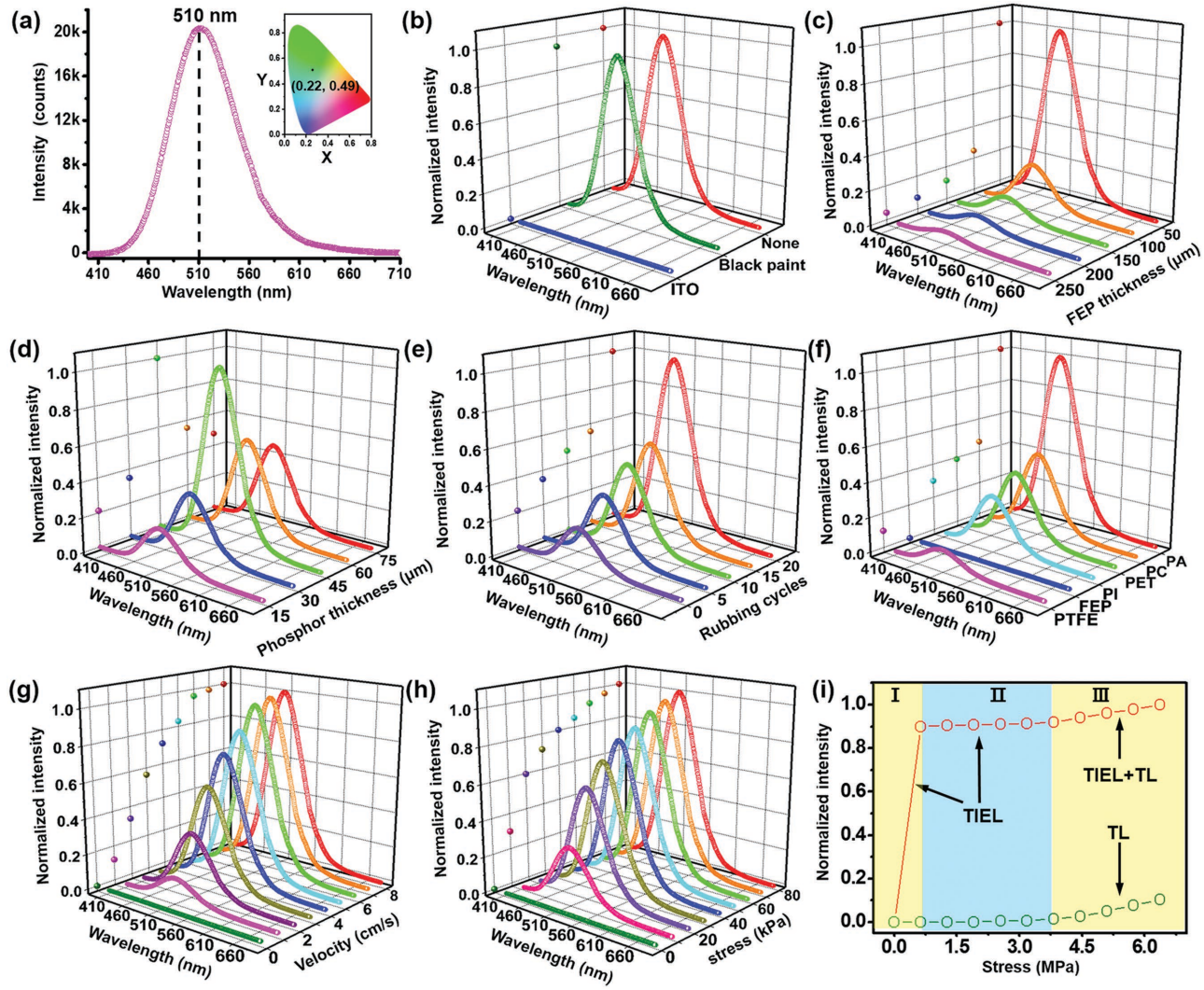

Figure 2. Experimental measurement results of the TIEL. a) Wavelength spectrum of the TIEL and its corresponding CIE coordinates. b) Wavelength spectra of control samples to identify possible luminescence mechanisms. c–h) Dependence of wavelength spectra on the thickness of the electrification layer, the thickness of the luminescent layer, the rubbing cycles, the materials of the sliding object, the sliding velocity, and the stress. i) Luminescence intensity of the TIEL and the conventional TL in distinct stress regions.

This is because the sandpaper rubbing assists the generation of higher surface charge density (Figure S2a, Supporting Information). It can be then obtained that more sandpaper rubbing is very likely to create more interface contact area, although this pretreatment does reduce the surface roughness as revealed by the atomic force microscopy results in Figure S2f (Supporting Information). Subsequent systematic study may be needed to establish a quantitative correlation between the surface roughness and the luminescence intensity.

From the aspect of external conditions, the material of the sliding object is a primary factor. If the sliding object is made of a material that is identical to that of the electrification layer, i.e., FEP in this case, negligible luminescence can be obtained; whereas a dissimilar material results in observable luminescence. Shown in Figure 2f, as the material of the sliding object becomes increasingly positive in terms of "triboelectric series,"[30] i.e., from PI to polyamide, the luminescence intensity is enhanced. It is noticed that poly(tetrafluoroethylene) can also induce light emission although it is more triboelectric negative than FEP. This observation can be explained by the ac-driven characteristic or polarity independence of the EL.[18,19] The above material dependence of the luminescence intensity further validates the proposed mechanism of the TIEL and rules out other possible mechanisms, such as elastico-TL based piezophotonic effect.[31] Moreover, the velocity of the sliding object almost linearly relates to the luminescence intensity until saturation occurs when it is greater than 6 cm s^{-1}. In addition, the luminescence intensity largely depends on the stress at the contact surfaces. It is noticeable that even an extremely low stress (10 kPa) is sufficient to induce substantial luminescence, making the threshold stress at the order of kPa. The responsivity defined as $\Delta I/\Delta\sigma$, where ΔI is the variation of the luminescence intensity and $\Delta\sigma$ is the stress increment, is calculated to be 0.03 kPa^{-1} in a stress region below 20 kPa. If

the stress of a broader scale is applied as shown in Figure 2i, a three-section behavior of the luminescence intensity can be observed (top curve). In section I, the TIEL intensity rapidly increases; and it saturates in section II because of the saturation of the tribocharge density.[32] Further increase of the intensity in section III is attributed to the elastico-TL of the phosphor as the stress increases beyond 3.8 MPa, which is consistent with previous reports on the threshold stress of ZnS-based materials for TL.[31,33] The corresponding responsivity of the TL in Figure 2i is calculated to be 0.04 MPa^{-1}. In this regard, compared to the TL, the TIEL represents a threshold stress that is smaller by three orders of magnitude and a responsivity enhanced by 750 times. It can be further obtained that the luminescence from the TIEL and the TL can be superimposed, which strongly indicates the fundamental distinction between the two phenomenon. We also tested the control sample that has the extra ITO layer as shown in Figure 2b. The measured luminescence intensity is exhibited by the bottom curve in Figure 2i, in which only the TL can be observed in the large-stress region.

As for the repeatability and stability of the TIEL, cyclic and bending tests are conducted. The cyclic characteristic is measured when the sliding object repeatedly slides against the electrification layer in a reciprocating way (cyclic frequency: 1 Hz; sliding velocity: 6 cm s^{-1}; contact pressure: 60 kPa). The peak luminescence intensity of each cycle is recorded and as showed in **Figure 3**a. After 20 000 cycles, the luminescence intensity only slightly drops by less than 5%, demonstrating good repeatability. The flexing/bending stability is shown Figure 3b. As the bending curvature increases from 0 to 100 m^{-1}, the variation of the luminescence intensity is less than 5%, demonstrating not only good robustness against bending but also potential applications of the TIEL on curved surfaces.

To well understand the measured data in depth, we conducted theoretical analysis *via* analytical calculation as well as numerical simulation. The EL of the powder-based ZnS:Cu phosphor is normally attributed to acceptor-type luminescence.[34,35] The excited electrons in the shallow electron trap states fall into the states of Cu impurity, which generates luminescence at a wavelength of 510 nm through recombination,[36,37] as illustrated in **Figure 4**a. The expected wavelength is in great consistence with the experimentally measured data. It is well established that the surface of the moving object is immediately charged once it contacts with the electrification layer. As the sliding occurs, the tribocharge density on the moving object would quickly reach a saturated value that is material dependent.[38] This statement is supported by our measured surface electric potential on the electrification layer shown in Figure 4b. Before sliding, the background surface potential along the preset sliding trajectory was found to be zero in average. The very minor fluctuation may result from charged particles absorbed from the air. In the early stage of the sliding, the surface potential is significantly raised due to the accumulation of tribocharges, suggesting substantial charge transfer at the contact surfaces. Subsequently, the surface potential sharply drops as the sliding continues and merges into the background after sliding for 2 cm, which indicates that tribocharges no longer form on the electrification

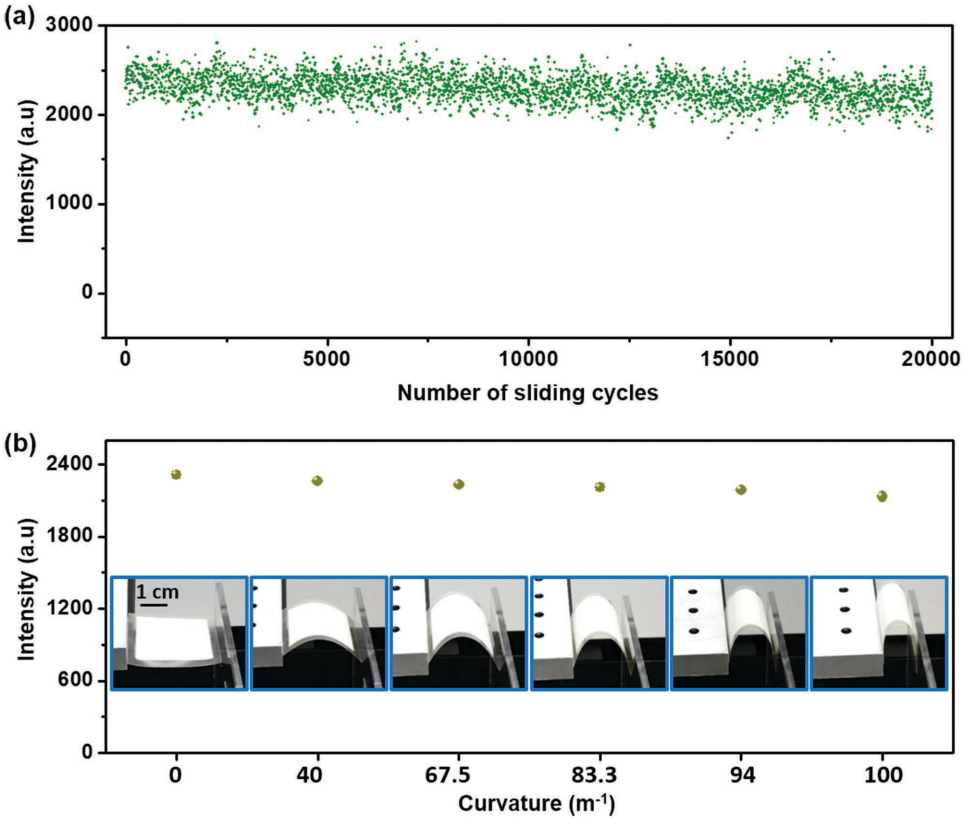

Figure 3. The repeatability and stability of the TIEL. a) The TIEL cyclic characteristic during 20 000 sliding cycles. b) The bending stability of the luminescence intensity with increasing bending curvature.

Adv. Mater. **2016**,
DOI: 10.1002/adma.201600604

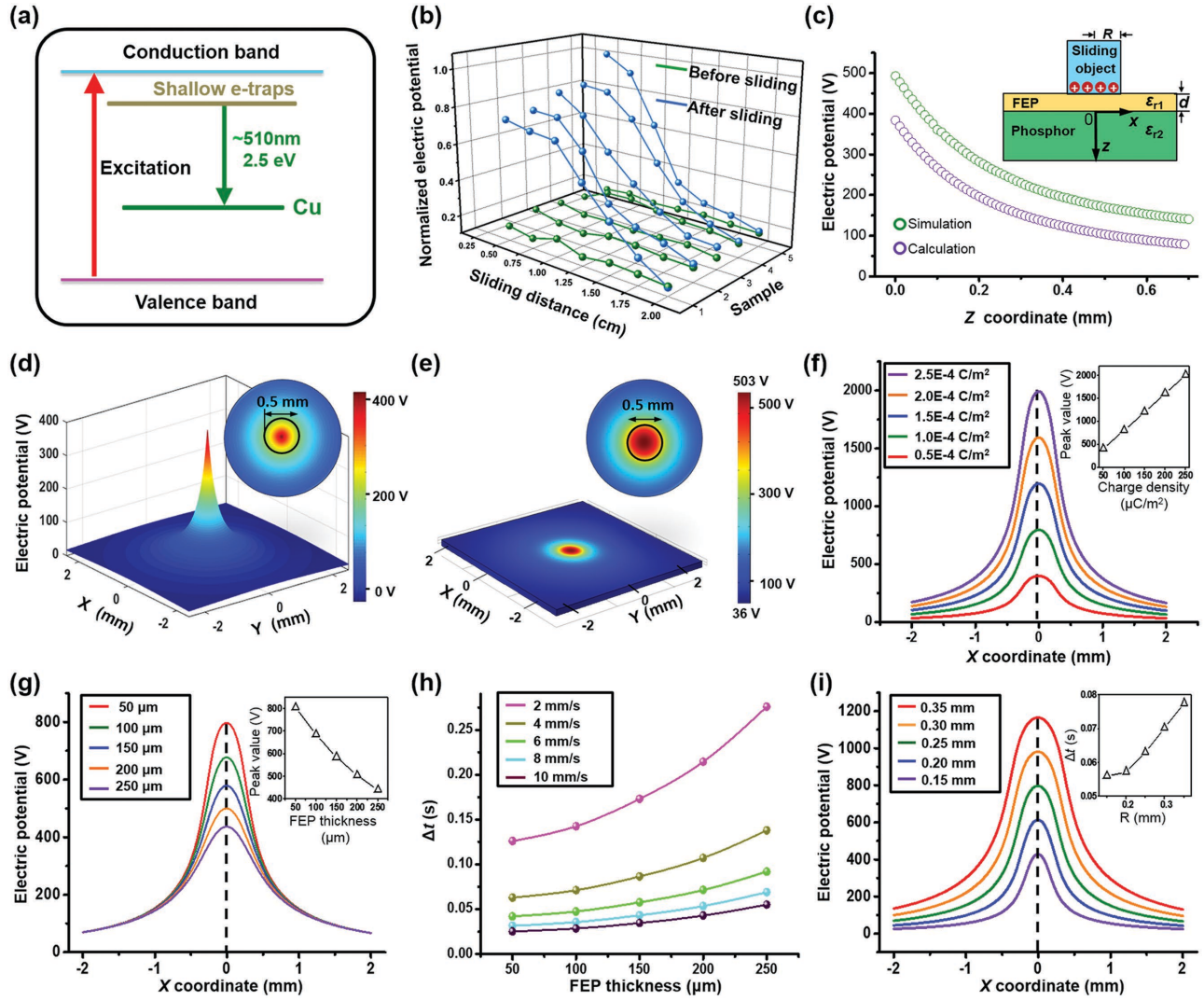

Figure 4. Theoretical analysis of the TIEL. a) Band diagram of the EL of ZnS:Cu phosphor. b) Surface electric potential on the electrification layer along the sliding trajectory before and after the sliding. c) Electric potential along the thickness of the luminescent layer by calculation and simulation, inset: 2D structural diagram. Electric potential distribution in two dimensions derived from the analytical solution d) and from the numerical simulation e) insets: top-down views. f) 1D electric potential distribution affected by surface tribocharge density on the sliding object, inset: dependence of the electric potential amplitude on the tribocharge density. g) 1D electric potential distribution affected by the thickness of the electrification layer, inset: dependence of the electric potential amplitude on the thickness. h) Dependence of the Δt on the thickness of the electrification layer at different sliding velocities. i) 1D electric potential distribution influenced by the radius of the sliding object, inset: dependence of the Δt on the radius.

layer. Considering the short distance needed before the charge saturation, we can reasonably assume that the electrification layer is charge free and that the sliding object carries a constant tribocharge density in the following theoretical analysis.

Underneath the charged sliding object, the electric potential in the phosphor layer along the thickness direction, i.e., z-axis in the inset of Figure 4c, can analytically expressed by the Equation (1). The detailed derivation process is presented in Note S1 (Supporting Information).

$$U(z)-U(0)=\frac{\sigma}{2\varepsilon_0\varepsilon_{r2}}\left(\sqrt{(z+d)^2+R^2}-z-d\right)+\left(\frac{\sigma}{2\varepsilon_0\varepsilon_{r1}}-\frac{\sigma}{2\varepsilon_0\varepsilon_{r2}}\right)\sqrt{d^2+R^2}-\frac{\sigma}{2\varepsilon_0\varepsilon_{r1}}(R+d)+\frac{\sigma}{2\varepsilon_0\varepsilon_{r2}}d \quad (1)$$

where $U(z)$ is the electric potential along the thickness of the luminescent layer, $U(0)$ is the electric potential of the reference point, σ is the saturated tribocharge density on the sliding object, ε_0 is the vacuum permittivity, ε_{r1} is the relative permittivity of the electrification layer, ε_{r2} is the relative permittivity of the luminescent layer, d is the thickness of the electrification layer, z is the distance into the luminescent layer (inset of Figure 4c), and R is the radius of the sliding object. Using the known parameters, i.e., $\sigma = 10^{-14}$ C m^{-2},[39] $\varepsilon_{r1} = 2.1$, $\varepsilon_{r2} = 2.9$, $R = 0.25$ mm, and $d = 0.05$ mm, we can obtain the analytical solution of the electric potential as follows:

$$U(z)=1948\left(\sqrt{(z+0.05)^2+0.25^2}-z-0.05\right) \quad (2)$$

Plotted in Figure 4c, the electric potential up to hundreds of volts is created within the luminescent layer by the positively charged object. Numerical simulation via COMSOL gives another curve that is also drawn in Figure 4c. In comparison, the simulated data are slightly higher than the calculated ones by tens of volts. This discrepancy is likely to be attributed to the simplifications in the analytical model as discussed in Note S1 (Supporting Information). Because the top surface of the luminescent layer ($z = 0$) has the most significant electric potential variation, we will focus on the electric potential on the surface in the following discussion. The analytical solution of Equation (2) in two dimensions at $z = 0$ is plotted in Figure 4d. Within the perimeter of the sliding object, the electric potential reaches the maxima up to 400 V at the center (inset of Figure 4d), whereas it drastically drops outside of the perimeter. The 2D electric potential distribution can be alternatively obtained by the numerical simulation via COMSOL which yields similar results shown in Figure 4e. Therefore, as the charged object slides over, the electric potential within the luminescent layer along the trajectory sharply increases and then immediately drops. This ac-like dynamic variation consequently excites the luminescence of the phosphor.

It is well established that the intensity of conventional ac-driven EL is primarily determined by two parameters, i.e., driving voltage and driving frequency.[40–42] Correspondingly in our case, the amplitude and the time span of the electric potential variation play the key roles in determining the luminescence intensity, respectively. In this regard, we adopt simulation results along the x-axis to theoretically explain how major factors influence the luminescence intensity. First, the tribocharge density on the sliding object is linearly related to the amplitude of the electric potential, as shown in Figure 4f. This result well explains the observations in Figure 2f that highly charged materials can generate strong luminescence. To validate the proposed simulation, the electric potential at the sliding interface is measured using Electrostatic Voltmeter Monroe 279. The electric potential is measured to be 700 V, and the surface charge density σ is derived to be 0.93×10^{-4} C m^{-2}. Based on our simulation results, given the surface charge density of 0.93×10^{-4} C m^{-2}, the simulated surface potential is 720 V as shown in Figure 4f, which is in excellent consistence with the measured data. Second, the thickness of the electrification layer has a dual effect on the luminescence intensity. On one hand, it affects the electric potential amplitude. As shown in Figure 4g, if the FEP thickness shrinks from 250 to 50 μm, the amplitude can be enhanced by 100% from 400 to 800 V. On the other hand, it also affects how fast the electric potential changes. To be quantitative, we define a parameter Δt that represents the time needed for the change of the electric potential by 200 V from the maxima. The decrease of the FEP thickness results in a shortened Δt, which is illustrated by individual curves in Figure 4h. Therefore, thinner electrification layer has twofold advantages, which is the reason for the measured exponential dependence of the luminescence intensity on the thickness in Figure 2c. Third, the sliding velocity is found to be inversely proportional to the Δt, as shown by a series of curves in Figure 4h. The simulation results are consistent to the measured data in Figure 2g. In addition, the diameter of the sliding object exerts two opposite effects on the luminescence intensity. Although increasing the diameter can promote the electric potential amplitude due to the weakened edge effect,[43,44] it results in a broadened electric potential distribution (Figure 4i) and thus a prolonged Δt (inset of Figure 4i). Therefore, there exists an optimal value of the diameter.

The TIEL enables light emission that has high intensity and high responsivity as a result of weak mechanical interactions, making it attractive in sensing and human–machine interfacing applications. Here we employed the layer-by-layer composite material to demonstrate real-time position locating and motion tracking in a visualized way. To achieve precise positioning, we designed and fabricated the luminescent layer into a segmented structure, as depicted in **Figure 5**a. The phosphor particles fill into an array of cells, which is shown in the magnified inset of Figure 5a. The elastomer-based composite film with the segmented structure is displayed in Figure 5b that demonstrates its bendable and twistable features. The cells shown in Figure 5c by SEM images are made from graphite-doped poly(dimethylsiloxane) (PDMS) with a height of 45 μm. When uniformly loaded with the phosphor particles, the cells segment the luminescent layer into an array of independent units (Figure 5d). The opaqueness of the cell walls blocks the lateral diffusion of the emitted luminescence to prevent cross-talk between adjacent cells. As a result, the position and the contour profile of the sliding object can be precisely revealed. The resolution of the segmented structure can be further promoted provided that phosphor of finer particle size is used. The detailed flow of the fabrication process is illustrated in Figure S3 (Supporting Information) and also presented in the Experimental Section.

An image acquisition system for the demonstration is depicted in Figure 5e, a camcorder was employed to capture the luminescence induced by the sliding object. A two-window software interface was programmed to display the live image as well as the overall trajectory of the luminescence. As a capital letter "B" is being written by a pen-like object with a fine tip of 1 mm in diameter, a series of live recorded images of consecutive frames are exhibited at an interval of 0.25 s in Figure 5f. When combined and superimposed together, the separate frames yield an overall trajectory of a complete letter "B" in Figure 5g. After data processing *via* MatLab, a quantitative mapping of the luminescence intensity can be obtained, which is presented in Figure 5h. It can be explicitly observed that the luminescence intensity considerably varies along the trajectory because the applied force as well as the velocity significantly varies during writing. For example, along the dashed line defined in Figure 5g, the luminescence intensity at the positions of "1" and "2" has clear distinctions (Figure 5i). The visualized handwriting of a string of letters can be achieved either by a fine-point contact, i.e., the word "light" and its corresponding Chinese character (Figure 5j and Movie S1, Supporting Information), or by a plane contact of 5 mm in diameter that induces luminescence in a large area (Figure 5k and Movie S2, Supporting Information). This unique feature of the large-area light emission again distinguishes the TIEL from the conventional TL. The segmented structure is proved to promote the spatial resolution. The visual trajectory of a sliding object (1 mm in diameter) and its corresponding intensity distribution are exhibited in Figure 5l, while the same set of data from a composite film without the

Adv. Mater. **2016**,
DOI: 10.1002/adma.201600604

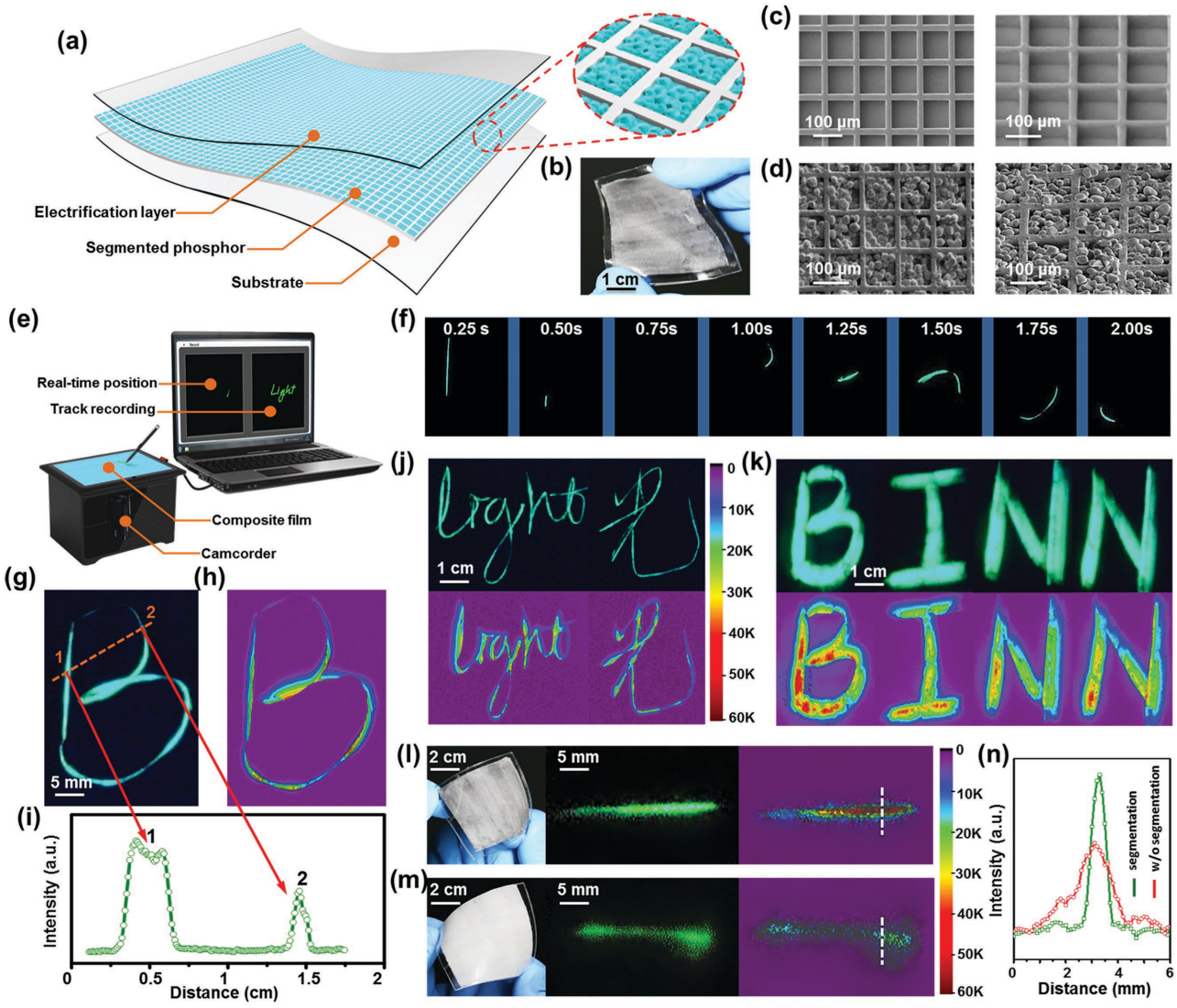

Figure 5. Demonstration of the TIEL in sensing applications. a) Schematic diagram of the composite material with the segmentation structure in the luminescent layer, inset: magnified view of the segmentation structure. b) Photograph of a twisted composite material. c) SEM images of the empty cells made from graphite-doped PDMS, left section: top-down view, right section: tilted view with 45° of angle. d) SEM images of cells filled in with phosphor particles, left section: top-down view, right section: tilted view with 45° of angle. e) Image acquisition system for the demonstration. f) Live images captured by the camcorder in consecutive frames at an interval of 0.25 s. g) Superimposed image showing the complete trajectory of a letter "B." h) Luminescence intensity mapping after being processed by MatLab. i) Luminescence intensity distribution along the dashed line defined in (g). j) A continuous trajectory showing a word "light" and its Chinese character, top section: live luminescence image, bottom section: corresponding mapping of the luminescence intensity. k) Luminescence induced by a large-area object, top section: live luminescence image, bottom section: corresponding mapping of the luminescence intensity. l) TIEL from the composite material having the segmentation structure, left section: photograph of the composite film, middle section: live luminescence image, right section: corresponding mapping of the luminescence intensity. m) TIEL from the composite material without the segmentation structure, left section: photograph of the composite film, middle section: live luminescence image, right section: corresponding mapping of the luminescence intensity. n) Luminescence intensity distribution along the dashed lines defined in (l) and (m).

segmentation is presented in Figure 5m. The luminescence intensity distribution along the dashed lines in Figure 5l,m is shown in Figure 5n. It is found that the light emission from the segmented sample is well confined and has a concentrated intensity at the center. The clear-cut boundary has a width of 1 mm that matches well with the diameter of the sliding object. Consequently, the position and the contour profile of the sliding object can be precisely derived. In comparison, the luminescence from the sample without the segmentation laterally diffuses without a distinct boundary (Figure 5n). Demonstration of the handwriting shown in this work is promising to be used in "smart writing". The characteristic distribution of the luminescence intensity can reflect the unique habits of a person's handwriting. As a result, it adds an extra criterion to signature recognition and makes it more secure, which is valuable for applications including anti-counterfeiting and electronic commerce.

It is because of the unique advantages and merits discussed above that the TIEL is promising to be used in a variety of areas

in addition to the example of motion tracking as demonstrated above. It is suitable for uses in displays, image recognition, and security surveillance. Besides, because it can emit strong light in a large area, it can be applied in portable illumination without reliance on an external power source.

In summary, we report a novel triboelectrification-induced electroluminescence that converts dynamic motions into luminescence upon extremely week mechanical interaction without supplying an external power source. Tribocharges resulting from relative sliding motion between two dissimilar materials can abruptly and significantly alter the surrounding electric potential. As a result, electroluminescent phosphor along the motion trajectory can be excited. Compared with the conventional TL, the novel TIEL possesses prominent advantages, including excellent stability, extremely low stress threshold, and high responsivity. As a demonstration of potential applications, position locating and motion tracking in a high-spatial resolution is achieved. Therefore, the TIEL is a new approach for widespread applications including security surveillance, electronic commerce, anti-counterfeiting, and illumination.

Experimental Section

Fabrication Process of a Flexible Multilayered Composite Material: A layer of transparent PI film of 100 μm thickness was cut into 5 cm × 5 cm pieces as a flexible substrate. Scotch tape of 45 μm in thickness was adhered along the two opposite edges of the substrate. The ZnS:Cu phosphor particles were mixed with the PMMA matrix at a mass ratio of 5:1 to form a paste. Such a ratio was optimized to achieve high luminescence intensity, as well as to form a coherent composite material. The phosphor paste was applied to the substrate and it was thinned by scraping along the scotch tape using a razor blade. The paste was dried and cured in an oven at 130 °C for 15 min. A layer of FEP of 50 μm in thickness was applied as an electrification layer.

Fabrication Process of a Composite Material with the Segmented Structure: A silicon wafer was rinsed with acetone, isopropyl alcohol, and ethyl alcohol in sequence. A layer of photoresist (Suntific SUN-9i, negative photoresist, 60 mJ cm^{-2}) with a thickness of 4 μm was spin-coated at a spinning rate of 2000 r m^{-1} for 120 s. The sample was prebaked at 110 °C for 120 s. Patterned square windows were created on the photoresist with a unit side length of 100 μm and an interval of 20 μm by photolithography (SUSS MA6, 365 nm at a dose of 17 mJ cm^{-2} s^{-1}). The sample was postbaked at 140 °C for 90 s. The sample was developed (Suntific 238D) for 70 s. The silicon wafer was etched by inductive coupled plasma (NMC DSE200S, SF_6:130 sccm, O_2: 13 sccm, C_4F_8: 80 sccm, power: 600 W, bias: 100 V, pressure: 45 mTorr, time: 15 min) to form trenches with a depth of 45 μm. The residual photoresist was removed by rinsing with acetone for 60 s. Graphite powder (particle size: 5 μm) was added into PDMS (Dow Corning 184) with a mass ratio of 1:10. The graphite-doped PDMS was applied onto the etched side of the silicon wafer. The sample was baked at 120 °C for 1 h and then the graphite-doped PDMS was peeled off. The phosphor paste was applied onto the graphite-doped PDMS and it was thinned using a razor blade. The sample was baked at 130 °C for 15 min. A thin layer of FEP film (50 μm) was adhered onto the flexible segmented PDMS structure.

Supporting Information

Supporting Information is available from the Wiley Online Library or from the author.

Acknowledgements

X.Y.W. and G.Z. contributed equally to this work. This research was supported by the Chinese "Thousands Talents" program for pioneer researcher and by the National Science Foundation of China (Grant No. 51572030).

Received: January 31, 2016
Revised: March 18, 2016
Published online:

[1] C. G. Camara, J. V. Escobar, J. R. Hird, S. J. Putterman, *Nature* **2008**, *455*, 1089.
[2] E. Ducrot, Y. Chen, M. Bulters, R. P. Sijbesma, C. Creton, *Science* **2014**, *344*, 186.
[3] E. Boldyreva, *Chem. Soc. Rev.* **2013**, *42*, 7719.
[4] X. Wang, C.-N. Xu, H. Yamada, K. Nishikubo, X.-G. Zheng, *Adv. Mater.* **2005**, *17*, 1254.
[5] S. S. Babu, M. J. Hollamby, J. Aimi, H. Ozawa, A. Saeki, S. Seki, K. Kobayashi, K. Hagiwara, M. Yoshizawa, H. Mohwald, T. Nakanishi, *Nat. Commun.* **2013**, *4*, 1969.
[6] J. H. Yu, S.-H. Kwon, Z. Petrášek, O. K. Park, S. W. Jun, K. Shin, M. Choi, Y. Il Park, K. Park, H. B. Na, N. Lee, D. W. Lee, J. H. Kim, P. Schwille, T. Hyeon, *Nat. Mater.* **2013**, *12*, 359.
[7] H. Uoyama, K. Goushi, K. Shizu, H. Nomura, C. Adachi, *Nature* **2012**, *492*, 234.
[8] Z. An, C. Zheng, Y. Tao, R. Chen, H. Shi, T. Chen, Z. Wang, H. Li, R. Deng, X. Liu, W. Huang, *Nat. Mater.* **2015**, *14*, 685.
[9] S.-Y. Kwak, S. Yang, N. R. Kim, J. H. Kim, B.-S. Bae, *Adv. Mater.* **2011**, *23*, 5767.
[10] B. Xu, J. He, Y. Mu, Q. Zhu, S. Wu, Y. Wang, Y. Zhang, C. Jin, C. Lo, Z. Chi, A. Lien, S. Liu, J. Xu, *Chem. Sci.* **2015**, *6*, 3236.
[11] C. Feldmann, T. Justel, C. R. Ronda, P. J. Schmidt, *Adv. Funct. Mater.* **2003**, *13*, 511.
[12] H. Sun, N. Gao, K. Dong, J. Ren, X. Qu, *ACS Nano* **2014**, *8*, 6202.
[13] E. Bartolák-Suk, J. Imsirovic, H. Parameswaran, T. J. Wellman, N. Martinez, P. G. Allen, U. Frey, Béla Suki, *Nat. Mater.* **2015**, *14*, 1049.
[14] K. Saito, Y.-F. Chang, K. Horikawa, N. Hatsugai, Y. Higuchi, M. Hashida, Y. Yoshida, T. Matsuda, Y. Arai, T. Nagai, *Nat. Commun.* **2012**, *3*, 1262.
[15] K. Binnemans, *Chem. Rev.* **2009**, *109*, 4283.
[16] H. M. Shahbaz, K. Akram, J.-J. Ahn, J.-H. Kwon, *J. Agric. Food Chem.* **2013**, *61*, 4019.
[17] S. Ummartyotin, N. Bunnak, J. Juntaro, M. Sain, H. Manuspiya, *Solid State Sci.* **2012**, *14*, 299.
[18] Z.-G. Wang, Y.-F. Chen, P.-J. Li, X. Hao, J.-B. Liu, R. Huang, Y.-R. Li, *ACS Nano* **2011**, *5*, 7149.
[19] M. Bredol, H. S. Dieckhoff, *Materials* **2010**, *3*, 1353.
[20] P. F. Smet, I. Moreels, Z. Hens, D. Poelman, *Materials* **2010**, *3*, 2834.
[21] T. Zhai, L. Li, X. Wang, X. Fang, Y. Bando, D. Golberg, *Adv. Funct. Mater.* **2010**, *20*, 4233.
[22] S. Xiong, B. Xi, C. Wang, D. Xu, X. Feng, Z. Zhu, Y. Qian, *Adv. Funct. Mater.* **2007**, *17*, 2728.
[23] S. Kar, S. Chaudhuri, *J. Phys. Chem. B* **2005**, *109*, 3298.
[24] S. M. Jeong, S. Song, K.-I. Joo, J. Kim, S.-H. Hwang, J. Jeong, H. Kim, *Energy Environ. Sci.* **2014**, *7*, 3338.
[25] S. M. Jeong, S. Song, S.-K. Lee, N. Y. Ha, *Adv. Mater.* **2013**, *25*, 6194.
[26] S. M. Jeong, S. Song, S.-K. Lee, B. Choi, *Appl. Phys. Lett.* **2013**, *102*, 051110.
[27] H. T. Baytekin, A. Z. Patashinski, M. Branicki, B. Baytekin, S. Soh, B. A. Grzybowski, *Science* **2011**, *333*, 308.
[28] B. A. Grzybowski, A. Winkleman, J. A. Wiles, Y. Brumer, G. M. Whitesides, *Nat. Mater.* **2003**, *2*, 241.

[29] L. S. McCarty, G. M. Whitesides, *Angew. Chem., Int. Ed.* **2008**, *47*, 2188.
[30] Z. L. Wang, *ACS Nano* **2013**, *7*, 9533.
[31] X. Wang, H. Zhang, R. Yu, L. Dong, D. Peng, A. Zhang, Y. Zhang, H. Liu, C. Pan, Z. L. Wang, *Adv. Mater.* **2015**, *27*, 2324.
[32] Y. S. Zhou, Y. Liu, G. Zhu, Z.-H. Lin, C. Pan, Q. Jing, Z. L. Wang, *Nano Lett.* **2013**, *13*, 2771.
[33] B. P. Chandra, V. K. Chandra, P. Jha, *Appl. Phys. Lett.* **2014**, *104*, 031102.
[34] K. Manzoor, S. R. Vadera, N. Kumar, T. R. N. Kutty, *Appl. Phys. Lett.* **2004**, *84*, 284.
[35] W. Q. Peng, G. W. Cong, S. C. Qu, Z. G. Wang, *Opt. Mater.* **2006**, *29*, 313.
[36] A. A. Bol, J. Ferwerda, J. A. Bergwerff, A. Meijerink, *J. Lumin.* **2002**, *99*, 325.
[37] J. Wang, C. Yan, K. J. Chee, P. S. Lee, *Adv. Mater.* **2015**, *27*, 2876.
[38] X. Y. Wei, G. Zhu, Z. L. Wang, *Nano Energy* **2014**, *10*, 83.
[39] G. Zhu, J. Chen, T. Zhang, Q. Jing, Z. L. Wang, *Nat. Commun.* **2014**, *5*, 3426.
[40] B. Hu, D. Li, O. Ala, P. Manandhar, Q. Fan, D. Kasilingam, P. D. Calvert, *Adv. Funct. Mater.* **2011**, *21*, 305.
[41] V. Wood, M. J. Panzer, D. Bozyigit, Y. Shirasaki, I. Rousseau, S. Geyer, M. G. Bawendi, V. Bulovi, *Nano Lett.* **2011**, *11*, 2927.
[42] V. Wood, J. E. Halpert, M. J. Panzer, M. G. Bawendi, V. Bulovic, *Nano Lett.* **2009**, *9*, 2367.
[43] S. Niu, Y. Liu, S. Wang, L. Lin, Y. S. Zhou, Y. Hu, Z. L. Wang, *Adv. Mater.* **2013**, *25*, 6184.
[44] Y. Wu, Q. Jing, J. Chen, P. Bai, J. Bai, G. Zhu, Y. Su, Z. L. Wang, *Adv. Funct. Mater.* **2015**, *25*, 2166.